MATRIX DESIGN FOR STRATEGICALLY TUNED ABSOLUTELY RESILIENT STRUCTURES (STARS)

Thomas Lavin
President
Soems, Inc.
Watchung, NJ 07069

Houssam Toutanji
Professor of Civil Engineering
Department of Civil and Environmental Engineering
University of Alabama in Huntsville
Huntsville, AL 35899

Bo Xu
Graduate Research Assistant
Department of Civil and Environmental Engineering
University of Alabama in Huntsville
Huntsville, AL 35899

Teng K. Ooi
Adjunct Associate Professor
Department of Mechanical and Aerospace Engineering
University of Alabama in Huntsville
Huntsville, AL 35899

Kirk R. Biszick
Director of Engineering
Optechnology, Inc.
5000 Allendale Drive
Huntsville, AL 35811

John A. Gilbert
Professor of Mechanical Engineering
Department of Mechanical and Aerospace Engineering
University of Alabama in Huntsville
Huntsville, AL 35899

ABSTRACT

This paper discusses Strategically Tuned Absolutely Resilient Structures (STARS) and steps taken to improve their performance by developing lightweight, high-performance cementitious composites that rely on the interfacial bonding between the aggregate [Poly(vinyl butyral) (PVB)] and reinforcement [Poly(vinyl alcohol) (PVA) fiber]. PVB is selected because it is light weight, adheres well to a variety of surfaces, and has good energy-absorbing

characteristics. PVA fiber is used because it has a high tensile strength and bonds well with the cementitious matrix. We show that standard mortar techniques and components can produce relatively high strength flexible mortars without any hard aggregate at all. These mortars are not related to macro defect free cements which are usually prepared with very low w/c ratios and soluble polymers that do not act as aggregates; nor, are these mortars polymer concretes which use a cross linking polymer replacement for Portland cement.

A comprehensive trial and error mix design process was followed to arrive at a fiber-free baseline mix having a low density of 1548 kg/m^3 (96.6 lb/ft^3) and an average compressive strength of 40 MPa (5800 psi). Mechanical properties such as the compressive strength, flexural strength, ductility, fracture toughness, and impact resistance are evaluated as fibers are added. Results show that the compressive strength decreases slightly with increasing fiber volume fraction whereas flexural strength, ductility, fracture toughness, and impact resistance increase.

INTRODUCTION TO STARS

Strategically Tuned Absolutely Resilient Structures (STARS) represent a new generation of composites fabricated by placing a low modulus, lightweight matrix over multiple layers of a relatively stiff reinforcement [1]. Their ability to store and release energy depends upon a complex interaction between the shape, modal response, and the forcing function applied to drive the structure [2].

Although the designs are based on the strength, stiffness, and position of the materials in the composite section, matrix design is critical to the structural performance, since the overall design strategy relies on the large difference in stiffness between the constituents in the composite section to drive the internal stress from the matrix to the reinforcement. Since it is possible to produce a cementitious matrix that is more flexible than the polymeric matrices currently used to construct most advanced composite materials, STARS offer structural and aerospace engineers more design flexibility.

PRIOR RELATED RESEARCH IN STARS

The evolution of STARS [3] began with the production of thin, lightweight, and structurally efficient panels capable of resisting stresses produced by reverse bending [4]. The study showed that a very efficient composite structure could be fabricated by placing a flexible polymer-enhanced cementitious matrix having a relatively low elastic modulus over two layers of a rigid steel wire mesh having a relatively high elastic modulus. Materials were placed symmetrically to form an '"adaptive" section that reacted similarly when bending couples were reversed. Since the compressive strength of the cementitious material was less than its tensile strength [5], it was the modulus of elasticity and tensile strength of the cementitious matrix, as well as the bond strength between the matrix and the reinforcement, that impacted STARS design most.

A modified transform section theory was developed to determine the deflections and stresses in such highly compliant cementitious structures [6] and the method was applied to study graphite-reinforced composites. Multi-layered composite beams were analyzed by incorporating material properties established from standard tests and finite element modeling was used to verify results.

The work fueled another investigation that quantified the dynamic characteristics of laminated plates [7]. In this study, an analytical dynamic finite element model was developed to evaluate the natural frequencies and mode shapes for structures subjected to different boundary conditions. This model was subsequently applied to study the dynamic performance of a larger structure [8]. Numerical results compared favorably with experimental impact hammer test data. As a result, it was concluded that the classical laminated plate theory developed for composite materials could be applied to quantify the dynamic behavior of highly compliant composite structures made from cementitious materials. Finally, research performed on stiffer concretes showed that material deficiencies caused by impact could be overcome by introducing a stiff weave-like reinforcement [9], and a ballistic investigation was performed to characterize the impact properties of STARS [10].

In all of the studies described above, the reinforcement consisted of a bidirectional mesh fabricated from either steel or graphite. An alternative approach for reinforcing STARS is to reinforce the composite by adding chopped fibers. This paper outlines steps taken to explore this possibility.

LOOKING AT MATRIX DESIGN FROM A NEW PERSPECTIVE

Previous studies, involving interactions between the aggregate and matrix in cementitious composites, show that the interfacial transition zone (ITZ), which is characterized by the prevalence of calcium hydroxide and higher

porosity, is the weakest region in a concrete structure. Interactions in this zone drive many important macroscopic properties, such as strength, permeability, and durability [11].

Researchers studying the microstructure of the ITZ and the hydration progression into it, for example, have confirmed a wall effect [12-19]. They note that ions have a tendency to flow slightly faster near the wall because of the decreased permeability in this zone [20]. As a result, the space around the aggregates is less effectively filled by hydration products. At the same time, there is greater tendency for calcium hydroxide [CH ($Ca(OH)_2$)] and ettringite to develop in this space.

Methods have been studied to improve the aggregate/matrix bonding in the ITZ, such as reducing the size of the aggregates [21, 22], using basalt and quartzite as aggregates [23], or replacing the cement with ultrafine additions of constituents, such as silica fume and metakaolin [24-26]. However, these methods are limited in scope, since they do not significantly alter the nature of the interaction between aggregate and matrix.

Moreover, in addition to interactions within the aggregate/matrix interface, fiber/matrix debonding may occur due to mechanisms such as shear type deformation and fiber sliding [27]. Steel and glass fibers are typically added to reinforce the matrix because of their high tensile strength. But the bond strength between these traditional materials and the matrix is limited.

The methods for enhancing the strength at an interface and the philosophy for using the traditional materials described above originated prior to the development of nanotechnology and supramolecular chemistry. But these processes can be used to create new materials, devices, and systems at the molecular level by adjusting phenomena associated with atomic and molecular interactions that strongly influence macroscopic material properties [28]. Materials having the potential to form strong interactions at the molecular level have been developed and utilized to produce novel nanocomposites with enhanced properties [29-33].

WHY PVB AND PVA?

Both PVB and PVA contain hydroxyl groups that have the potential to form a hydrogen bond between molecules, or within different parts of a single molecule. This unique feature provides remarkable changes in the surface bond strength, not only between the aggregate and the matrix, but also between the fiber reinforcement and the matrix. Additionally the ether oxygen functional groups act as a weak base and could potentially interact with Lewis acids and electropositive materials such as CSH.

Poly(vinyl butyral) (PVB) is a member of the class of poly(vinyl acetal) resins [34]. It is derived by condensing poly(vinyl alcohol) (PVA) with butyraldehyde in the presence of a strong acid. PVA reacts with the aldehyde to form six-membered rings primarily between adjacent intramolecular hydroxyl groups, leading to the structure shown in Fig. 1. PVB aggregate is completely insoluble in cement-water-mixes and is highly alkali resistant.

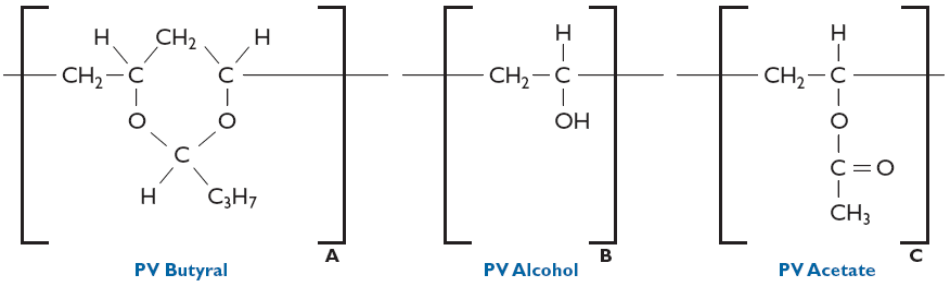

Figure 1. Structure of poly(vinyl butyral) (pvb) [34].

PVB is commercially prepared by a well-known reaction between aldehydes and alcohols. However, the resulting polymer is actually a terpolymer of PVB, polyvinyl alcohol (PVA), and polyvinyl acetate because of incomplete conversion. The presence of hydroxyl groups in the polymer molecule not only enables good wetting of most substrates, but also furnishes a reactive site for chemical combination with thermosetting resins. This is attributed to the hydroxyl groups in the PVB polymer that provide electrostatic attractive and hydrogen bonding interactions with other substances. PVB has a mixed hydrophobic hydrophilic nature, and aggregate surface availability will depend on the nature of the solvent it is within. The hydrophilic chemical interaction is illustrated in Fig. 2.

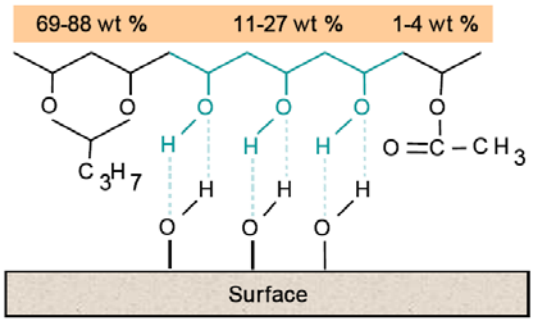

Figure 2. Adhesion to substrates by hydrogen bond.

Poly(vinyl alcohol) (PVA) is obtained from poly(viny1 acetate) which is readily hydrolysed by treating an alcoholic solution with an aqueous acid or alkali [35], leading to the structure shown in Fig. 3. PVA is a white powder with a specific gravity in the range of 1.2-1.3 and a glass transition temperature of around 80 ºC [36].

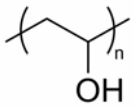

Figure 3. Structure of poly(vinyl alcohol) (PVA).

There are two main reasons for considering PVA fiber as a reinforcing material; namely, the mechanical properties of the fiber and their ability to bond well with a cementitious matrix. As illustrated in Table 1, the fiber has a high tensile strength, a high modulus, and low specific weight [35].

Table 1. Mechanical properties of PVA fibers.

Tensile Strength (MPa)	Elastic Modulus (MPa)	Specific Gravity
1.23×10^3	2.95×10^4	1.3

Wang and Li [37] reported that the hydrophilic nature of PVA fibers cause them to bond well with the cementitious matrix. The formation of this microstructure is attributed to the effect that PVA has on the nucleation of CH and C-S-H at the fiber surface and on the presence of polymer around the fibers.

CONSTITUENTS

A comprehensive trial and error mix design process was followed to arrive at a baseline mix (Mix No. M1 in Table 2) satisfying the basic criteria for STARS (high strength, low density, and low modulus). Then, three other mixes were placed (M2, M3, and M4) with the same water to cement ratio (w/c) and progressively higher fiber volume fractions, V_f (0.3%, 0.6%, and 0.9%, respectively). Specimens were prepared and tests conducted to study how different fiber volume fractions affected the compressive strength, flexural strength, ductility, fracture toughness, and impact resistance. All of the results presented later in the section labeled “Experimental Testing” reflect average values taken from three specimens.

Table 2. Mix proportions (kg/m^3).

Mix No.	Cement	Metakaolin	Water	SIKA	B 79	M B75H	PVA fiber	w/c	V_f (%)
M1	833.3	79.4	363.5	11.9	182.5	119.0	0	0.4	0
M2	833.3	79.4	363.5	11.9	182.5	119.0	4.2	0.4	0.3
M3	833.3	79.4	363.5	11.9	182.5	119.0	8.3	0.4	0.6
M4	833.3	79.4	363.5	11.9	182.5	119.0	12.5	0.4	0.9

Referring to Table 2, from left to right: the cement was ASTM Type I normal Portland cement conforming to ASTM C150 [38]; Metakaolin (MK) conformed to ASTM C618 [39]; and, the Sika ViscoCrete 2100 superplasticizer conformed to ASTM C494 [40].

The Poly(vinyl butyral) (PVB) added to each mix consisted of a combination of Butvar B-79 and Mowital B75H. Butvar B-79 is manufactured by Solutia Inc.; Mowital is produced by Kuraray Specialities Europe (KSE). Table 3 highlights selected properties of these PVB products.

Table 3. Selected properties of PVB products.

Property	Units	Designation	Value
PVOH* content	%	B-79	11.5-13.5
		M-B75H	11-27
Specific gravity	-	B-79	1.083
		M-B75H	1.1
Tensile yield strength	MPa	B-79	40-47
		M-B75H	
Elastic modulus	MPa $\times 10^3$	B-79	1.93-2.0
		M-B75H	
Impact strength	J m^{-1}	Izod notched (1.25 cm × 1.25 cm); B-79	42.7
		M-B75H	-
Glass transition temperature	ºC	B-79	62-72
		M-B75H	73

* PVOH is the polyvinyl alcohol (PVA) residual in the PVB polymer.

The poly(vinyl alcohol) (PVA) fibers used were manufactured by Kuraray Co. Ltd of Japan. They are classified by the manufacturer as RECS15 and have the properties listed in Table 4.

Table 4. Physical and mechanical properties of PVA fiber.

Fiber Type	Diameter (mm)	Thickness (dtex)	Cut Length (mm)	Tensile Strength (N/mm^2)	Elongation (%)	Modulus (kN/mm^2)	Specific Gravity
RECS15	0.04	15	8	1600	7	40	1.3

EXPERIMENTAL TESTING

Compressive Strength of Baseline Mix

Compressive strength was measured by testing 50 mm diameter 100 mm long (2 in. diameter x 4 in. long) cylinders at a constant loading rate of 20 MPa/min (2901 psi/min) following ASTM C39 [41]. Figure 4 shows a plot of the compressive strength of the baseline mix (M1) with time. It is observed that the strength increases slightly up to 60 days, after which the change is insignificant.

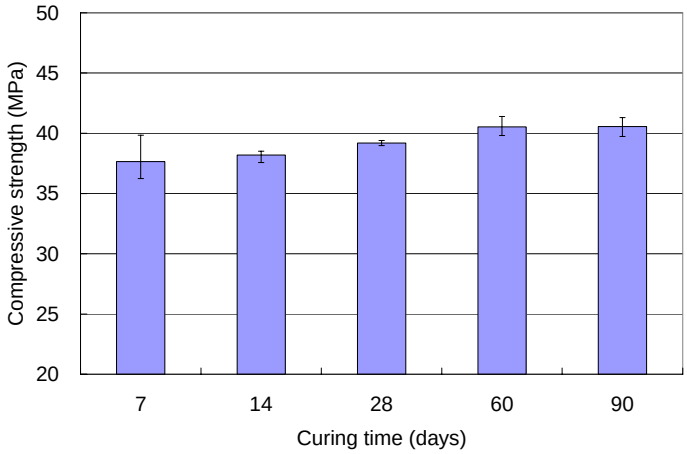

Figure 4. Compressive strength of PVB concrete with no fibers added.

Effect of PVA Fibers on Compressive Strength

The data listed in Table 5 shows that specimens without PVA fibers (M1) have an average compressive strength of 37.7 MPa (5461.4 psi) based on a 7 day cure. By comparison, the specimens placed with PVA fibers at a fiber volume fraction equal to 0.6% (M3), have an average compressive strength of 34.2 MPa (4896.2 psi) over the same period. It can be concluded that the addition of the fibers reduces the compressive strength by about ten percent.

Table 5. Compressive strength and density.

Mix No.	No. Specimens	V_f (%)	Compressive Strength (MPa)	Density (kg/m^3)
M1	3	0	37.7±1.56	1548.2±3.90
M3	3	0.6	34.2±0.14	1540.0±7.30

This slight reduction is attributed to the fact that the free fibers are randomly oriented thereby reducing their ability to resist compressive loads. They take up space and this reduces the effective bearing surface over which the applied load is distributed. Note that the average density of the specimens with PVA fibers was 1540.0 kg/m^3 (96.1 lb/ft^3), slightly lower than that of the specimens without them.

Effect of PVA Fibers on Flexural Strength and Ductility

As illustrated in Fig.5, the flexural strength was measured, in accordance with ASTM C1609 [42], by placing test specimens in third point bending. The specimens, which measured 70×25×210 mm (2.75x1x8.25 in.), were loaded at a rate of 667 N/min (150 lb/min), corresponding to a stress increase at the bottom surface (tensile side of the beam) of 1.72 MPa/min (250 psi/min).

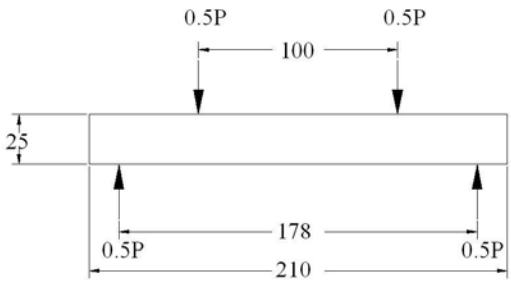

Figure 5. Experimental set up for third point bending (mm).

Figure 6 shows the flexural stress-strain plots for beams without (M1) and with fibers included at a fiber volume fraction equal to 0.6% (M3). Strain measurements were made on the top (compressive side of the beam) and bottom surfaces using strain gages.

Referring to Fig. 6, specimens without fibers reached an average ultimate stress of about 2.59 MPa (375 psi), the average strains at failure were -0.0006 and 0.0055 at the top and bottom, respectively. Specimens with fibers reached a higher average ultimate stress of 4.69 MPa (680 psi); the average strains at failure were -0.001 and 0.018 at the top and bottom of the beam, respectively. From these results, it can be concluded that the addition of fibers significantly improves the flexural strength. Since the beams with fibers were much stronger, and the compressive strength of a fiber-free matrix was observed to decrease when fibers were added, it can be inferred that the addition of fibers significantly increases the tensile strength of the matrix; albeit, this needs to be verified.

Toughness (ductility) is generally defined as the energy adsorption capacity and this parameter is calculated based on the area under a load-displacement curve. Figure 7 shows the load-displacement curves generated for the bending specimens placed with the two mixes described above. Referring to Fig 5, displacements were measured at the center of the beam relative to the upper supports. Table 6 contains relevant data.

The flexural toughness was computed by integrating the area under the curves up to the point of collapse. The toughness of the mix with no fibers was around 350 N-mm while that of the mix with fibers was about 1883 N-mm; thereby demonstrating that the addition of fibers markedly improves ductility (by more than 400%).

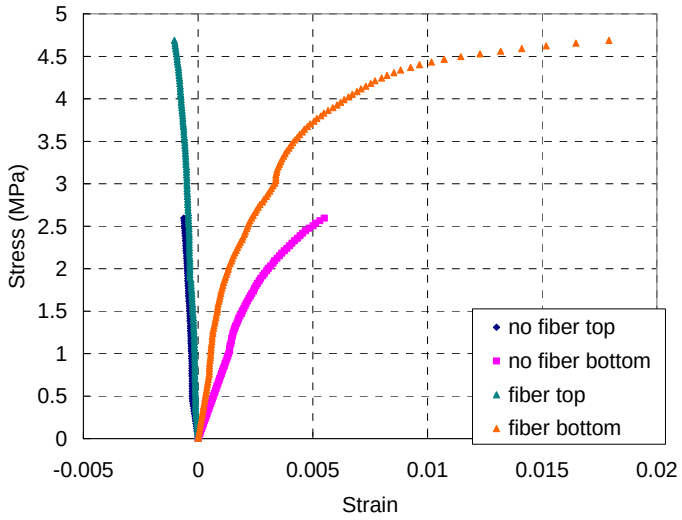

Figure 6. Flexural stress-strain plots for PVB concrete specimens.

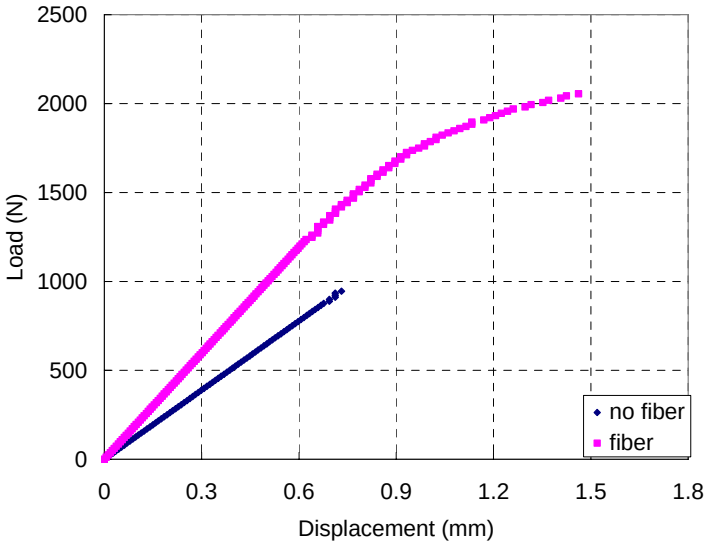

Figure 7. Flexural load-displacement plots for PVB concrete specimens.

Table 6. Flexural toughness.

Mixture	No. Specimens	V_f (%)	Load (N)	Displacement (mm)	Flexural Toughness (N-mm)
M1	3	0	932±16	0.75±0.1	350±0.8
M3	3	0.6	2093±105	1.64±0.1	1883±5.3

The improvement in flexural strength is attributed to the reinforcing effect created by the PVA fibers. Figure 8 shows a photograph of the fracture surface in a specimen that contained fibers. Many of the fibers remained intact, indicating that they pulled away from the matrix, as opposed to rupturing along their length.

Figure 8. Fibers remain intact along the fracture surface.

Effect of PVA Fibers on Fracture Toughness

Fracture toughness tests were performed on single edge notch bending (SENB) specimens following ASTM E399 [43]. As illustrated to the left in Fig. 9, the test specimens measured 23×46×203 mm (0.9x1.8x8.0 in.). They had a notch height to beam height (a/W) ratio equal to 0.5 and a free span to beam height ratio of 4.0. Referring to the photograph shown to the right in Fig. 9, specimens were tested in three-point bending, at a loading rate of 33 MPa-$m^{0.5}$/min (30 ksi-$in^{0.5}$/min).

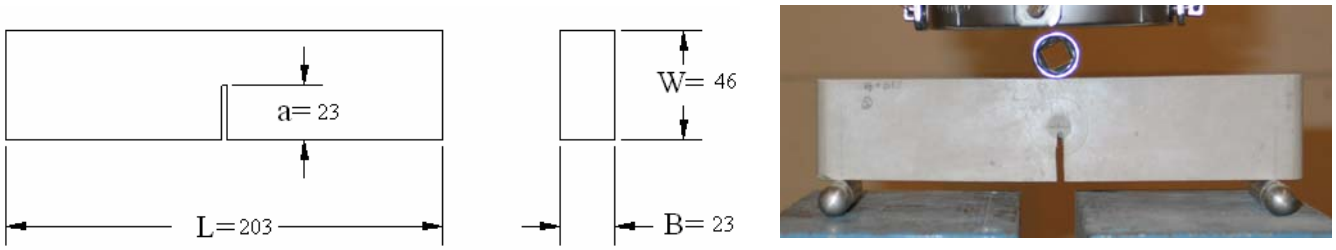

Figure 9. Single edge notch bending (SENB) PVB concrete specimens (mm).

Table 7 and Fig. 10 show data and a plot, respectively, of the fracture toughness obtained for specimens having progressively higher fiber volume fractions. It is evident that the fracture toughness increases linearly with the fiber volume fraction, resulting in improvements ranging from 37% to 108%. Visual inspection of the fracture surfaces indicated behavior similar to that observed during the flexural test where the fibers pulled away from the matrix as opposed to rupturing along their length during failure.

Table 7. Fracture toughness.

Mix No.	No. Specimens	V_f (%)	Fracture Toughness (MPa-$m^{0.5}$)
M1	3	0	0.389±0.021
M2	3	0.3	0.528±0.061
M3	3	0.6	0.691±0.077
M4	3	0.9	0.800±0.134

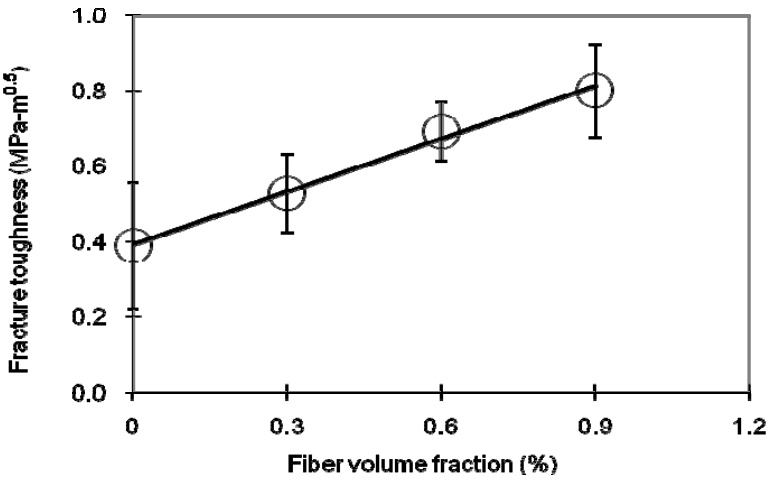

Figure 10. Fracture toughness for PVB concrete specimens.

Effect of PVA Fibers on Impact Resistance

Charpy V-notch tests were conducted following ASTM E23 [44]. Figure 11 includes the dimensions of the specimens tested while Fig. 12 shows the Tinius Olsen "Change-O-Matic" impact testing machine used to perform the tests.

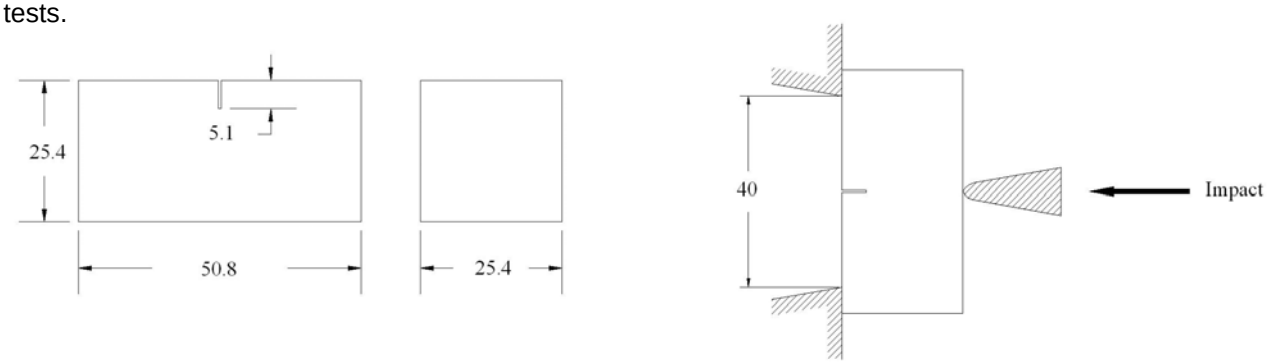

Figure 11. Charpy V-notch specimen (left) and loading configuration (right) (mm).

Figure12. Tinius Olsen "Change-O-Matic" impact testing machine.

After positioning the specimen, the pendulum is released from a height, y_1, and swings through the specimen to a height, y_2. Assuming negligible friction and aerodynamic drag, the energy absorbed by the specimen is equal to the height difference times the weight of the pendulum.

Table 8 and Fig. 13 show data and a plot, respectively, of the average impact energy obtained for specimens having progressively higher fiber volume fractions. It is evident that the impact energy dramatically increases when the fiber volume fraction reaches 0.9%.

Table 8. Impact resistance.

Mix No.	No. Specimens	V_f (%)	Impact energy (J-m^{-1})
M1	3	0	214.6±4.9
M2	3	0.3	231.8±10.0
M3	3	0.6	261.1±13.2
M4	3	0.9	458.1±49.2

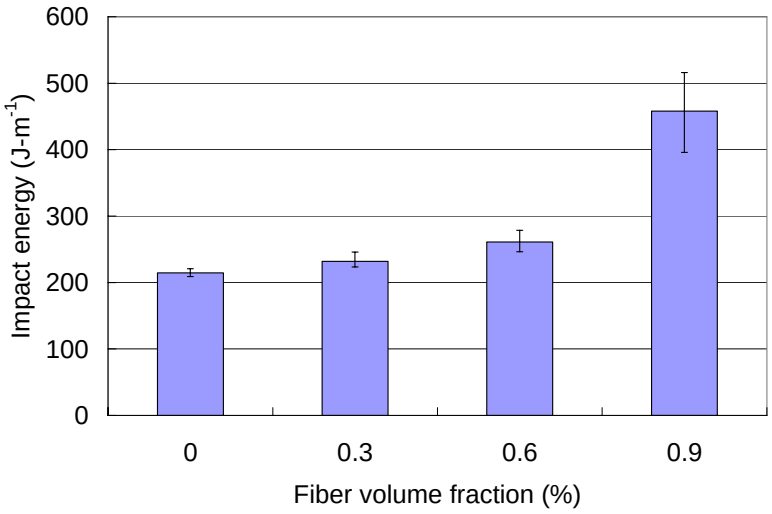

Figure 13. Impact energy for PVB concrete specimens.

CONCLUSIONS

This paper explores a new method for producing lightweight cementitious materials for STARS. The method relies on the interfacial bond developed between the aggregate (PVB) and reinforcement (PVA fiber) to improve mechanical properties such as tensile strength, ductility, fracture toughness, and impact resistance. Macro mechanical properties were tested and it was determined that the compressive strength of a baseline, placed with no fibers, increased with curing time; faster during the first 60 days, then only slightly after that.

The addition of PVA fibers decreases slightly the compressive strength but improves the flexural strength, ductility, fracture toughness, and impact resistance. The increase in fracture toughness was found to be linear with increasing fiber volume fraction; the increase associated with impact resistance was non-linear. The significant improvements in these parameters indicate that fibers play important roles in resisting dynamic loads.

REFERENCES

[1] Gilbert, J.A., Ooi, T.K., Biszick, K.R., Marotta, S.A., Vaughan, R.E., Engberg, R.C., “Strategically tuned absolutely resilient structures,” Proc. of SEM Annual Conference & Exposition on Experimental and Applied Mechanics, Portland, Oregon, June 7-9, 2005, Paper No. 222, 14 pages.

[2] Ooi, T.K., Engberg, R.C., Gilbert, J.A., Vaughan, R.E., Britton, H.L., “Modal analyses of polymer-enhanced, graphite reinforced cementitious composites,” Proc. of SEM Annual Conference & Exposition on Experimental and Applied Mechanics, Portland, Oregon, June 7-9, 2005, Paper No. 224, 11 pages.

[3] Biszick, K.R., Toutanji, H.A., Gilbert, J.A., Marotta, S.A, Ooi, T.K., “Evolution of strategically tuned absolutely resilient structures (STARS),” Proc. of SEM Annual Conference & Exposition on Experimental and Applied Mechanics, Saint Louis, Missouri, June 5-7, 2006, Paper No. 32, 7 pages.

[4] Biszick, K.R., Gilbert, J.A., “Designing thin-walled, reinforced concrete panels for reverse bending,” Proc. of the 1999 SEM Spring Conference on Theoretical, Experimental and Computational Mechanics, Cincinnati, Ohio, June 7-9, 1999, pp. 431- 434.

[5] Brara, A., Klepaczko, J.R., “Experimental characterization of concrete in dynamic tension,” CNERIB, Algeria and Laboratory of Physics and Mechanics of Materials, Ile de Saulcy, France (2005).

[6] Vaughan, R.E., Gilbert, J.A., "Analysis of graphite reinforced cementitious composites," Proc. of the 2001 SEM Annual Conference and Exposition, Portland, Oregon, June 4-6, 2001, pp. 532-535.

[7] Ooi, T.K., Gilbert, J.A., Bower, M.V., Vaughan, R.E., Engberg, R.C., “Modal analysis of lightweight graphite reinforced silica/polymer matrix composite plates,” Experimental Mechanics, 45(3): 1-5 (2005).

[8] Ooi, T.K., Engberg, R.C., Gilbert, J.A., Vaughan, R.E., Bower, M.V. “Modal testing of a lightweight cementitious structure,” Experimental Techniques, November/December: 37-40 (2004).

[9] Badr, A., Ashour, A.F., Platten, A.K., “Statistical variations in impact resistance of polypropylene fibre-reinforced concrete,” University of Central Lancashire, Preston, UK & University of Bradford, Bradford, UK (2005).

[10] Binek, L.A., Gilbert, J.A., Ooi, T.K., Bower, M.V., Biszick, K.R., “Ballistic testing of STARS,” Proc. of SEM Annual Conference & Exposition on Experimental and Applied Mechanics, Springfield, Massachusetts, June 3-6, 2007, Paper No. 196, 10 pages.

[11] Breton, D., Carles-Gibergues, A., Ballivy, G., Grandet, J., “Contribution to the formation mechanism of the transition zone between rock-cement paste,” Cement and Concrete Research, Vol. 23, pp. 335-346 (1993).

[12] Sun, Z., Garboczi, E.J., Shah, S.P., “Modeling the elastic properties of concrete composites: Experiment, differential effective medium theory, and numerical simulation,” Cement and Concrete Composites, Vol. 29, No. 1, pp. 22-38 (2007).

[13] Leemann, A., Münch, B., Gasser, P. Holzer, L., “Influence of compaction on the interfacial transition zone and the permeability of concrete,” Cement and Concrete Research, Vol. 36, No. 8, pp.1425-1433 (2003).

[14] Elsharief, A., Cohen, M.D., Olek, J., “Influence of aggregate size, water cement ratio and age on the microstructure of the interfacial transition zone,” Cement and Concrete Research, Vol. 33, No. 11, pp. 1837-1849 (2003).

[15] Nadeau, J. C., “Water-cement ratio gradients in mortars and corresponding effective elastic properties,” Cement and Concrete Research, Vol. 32, No. 3, pp. 481-490 (2002).

[16] Belaïd, F., Arliguie, G., François, R., “Porous structure of the ITZ around galvanized and ordinary steel reinforcements,” Cement and Concrete Research, Vol. 31, No. 11, pp. 1561-1566 (2001).

[17] Diamond, S., Huang, J.D., “The ITZ in concrete-a different view based on image analysis and SEM observations,” Cement and Concrete Composites, Vol. 23, No. 2-3, pp. 179-188 (2001).

[18] Harutyunyan, V.S., Abovyan, E.S., Monteiro, P.J.M., Mkrtchyan, V.P., Balyan, M.K., “Microstrain distribution in calcium hydroxide present in the interfacial transition zone,” Cement and Concrete Research, Vol. 30, No. 5, pp. 709-713 (2000).

[19] Scrivener, K.L., Nemati, K.M., “The percolation of pore space in the cement paste/aggregate interfacial zone of concrete,” Cement and Concrete Research, Vol. 26, No.1, pp. 35-40 (1996).

[20] Richard, J.S., “*Purifying Proteins for Proteomics: A Laboratory Manual*,” CSHL Press, Cold Spring Harbor, New York. p. 73 (2004).

[21] Akçaolu, T., Tokyay, M., Çelik, T., “Effect of coarse aggregate size on interfacial cracking under uniaxial compression,” Materials Letters, Vol. 57, No. 4, pp. 828-833 (2002).

[22] Akçaolu, T., Tokyay, M., Çelik, T., “Effect of coarse aggregate size and matrix quality on ITZ and failure behavior of concrete under uniaxial compression,” Cement and Concrete Composites, Vol. 26, No. 6, pp. 633-638 (2004).

[23] Tasong, W.A., Lynsdale, C.J., Cripps, J.C., “Aggregate-cement paste interface: Part I. Influence of aggregate geochemistry,” Cement and Concrete Research, Vol. 29, pp. 1019-1025 (1999).

[24] Bentz, D.P., “Influence of silica fume on diffusivity in cement-based materials. II. Multi-scale modeling of concrete diffusivity,” Cement and Concrete Research, Vol. 30, No. 7, pp. 1121-1129 (2000).

[25] Asbridge, A.H., Chadbourn, G.A., Page, C.L., “Effects of metakaolin and the interfacial transition zone on the diffusion of chloride ions through cement mortars,” Cement and Concrete Research, Vol. 31, No. 11, pp. 1567-1572 (2001).

[26] Poon, C., Lam, L., Kou, S.C., Wong, Y., Wong, R., “Rate of pozzolanic reaction of Metakaolin in high-performance cement pastes,” Cement and Concrete Research, Vol. 31, pp. 1301-1306 (2001).

[27] Friedrich, K., Fakirov, S., Zhang, Z., “*Polymer Composites: From Nano-to-Macro-Scale*,” Springer Inc., New York, pp. 129-130 (2005).

[28] Chong, K.P., “Nanoscience and engineering in mechanics and materials,” Journal of Physics and Chemistry of Solids, Vol. 65, pp. 1501-1506 (2004).

[29]Peng, Z., Kong L., Li, S., “Thermal properties and morphology of a poly(vinyl alcohol)/silica nanocomposite prepared with a self-assembled monolayer technique,” Journal of Applied Polymer Science, Vol. 96, No. 4, pp. 1436-1442 (2005).

[30] Piscevic, D., Tarlov, M. J., Knoll, W., “Surface plasmon microscopy of biotin-streptavidin binding reactions on UV-photopatterned alkanethiol self-assembled monolayers,” Supramolecular Science, Vol. 2, pp. 99-106 (1995).

[31] Yang, G., Gong, J., Yang, R., Guo, H., Wang, Y., Liu, B., Dong, S., “Modification of electrode surface through electrospinning followed by self-assembly multilayer film of polyoxometalate and its photochromic,” Electrochemistry Communications, Vol. 8, No. 5, pp. 790-796 (2006).

[32] Peng, Z., Kong L.X., Li, S.D., Spiridonov, P., “Polyvinyl alcohol/silica nanocomposite: its morphology and thermal degradation kinetics,” Journal of Nanoscience and Nanotechnology, Vol. 12, pp.393-340 (2006).

[33] Peng, Z., Kong, L.X., Li, S.D., “Non-isothermal crystallisation kinetics of self-assembled polyvinylalcohol/silica nano-composite,” Polymer, Vol. 46 pp. 1949-1952 (2005).

[34] Mark, J.E., “*Polymer Data Handbook*,” Oxford University Press, Inc., pp. 910-912 (1999).

[35] Zheng, ZH., Feldman, D., “Synthetic fiber-reinforced concrete,” Progress in Polymer Science., Vol. 20, pp. 185-210 (1995).

[36] Feldman, D., Barbalata, A., “*Synthetic Polymers: Technology, Properties, Applications, Chapman and Hall*,” London, pp.101 (1996).

[37] Wang, SX., Li, V.C., “Polyvinyl alcohol fiber reinforced engineered cementitious composites: material design and performances,” Proc. International RILEM Workshop on High Performance Fiber Reinforced Cementitious Composites in Structural Applications RILEM Publications SARL, In: Fischer, G., and Li, V.C. editors, RILEM Publications SARL, pp. 65-73 (2006).

[38] ASTM C150-07, Standard Specification for Portland Cement.

[39] ASTM C618-05, Standard Specification for Coal Fly Ash and Raw or Calcined Natural Pozzolan for Use in Concrete.

[40] ASTM C494-08, Standard Specification for Chemical Admixtures for Concrete.

[41] ASTM C39-05, Standard Test Method for Compressive Strength of Cylindrical Concrete Specimens.

[42] ASTM C1609-07, Standard Test Method for FLEXURAL Performance OF Fiber-Reinforced Concrete (Using Beam with Third-Point Loading).

[43] ASTM E399-06, Standard Test Method for Linear-Elastic Plane-Strain Fracture Toughness K_{Ic} of Metallic Materials.

[44] ASTM E23-07, Standard Test Methods for Notched Bar Impact Testing of Metallic Materials.